J. Fluid Mech. (1990), *vol.* 220, *pp.* 397–411
Printed in Great Britain

The structure of two-dimensional separation

By LAURA L. PAULEY[1], PARVIZ MOIN[2] AND WILLIAM C. REYNOLDS[2]

[1]The Pennsylvania State University, University Park, PA 16802, USA
[2]Stanford University, Stanford, CA 94305, USA
and NASA/Ames Research Center, Moffett Field, CA 94035, USA

(Received 19 June 1989 and in revised form 17 April 1990)

The separation of a two-dimensional laminar boundary layer under the influence of a suddenly imposed external adverse pressure gradient was studied by time-accurate numerical solutions of the Navier–Stokes equations. It was found that a strong adverse pressure gradient created periodic vortex shedding from the separation. The general features of the time-averaged results were similar to experimental results for laminar separation bubbles. Comparisons were made with the 'steady' separation experiments of Gaster (1966). It was found that his 'bursting' occurs under the same conditions as our periodic shedding, suggesting that bursting is actually periodic shedding which has been time-averaged. The Strouhal number based on the shedding frequency, local free-stream velocity, and boundary-layer momentum thickness at separation was independent of the Reynolds number and the pressure gradient. A criterion for onset of shedding was established. The shedding frequency was the same as that predicted for the most amplified linear inviscid instability of the separated shear layer.

1. Introduction

Boundary-layer separation occurs in many practical problems. It is important to know the conditions under which separation occurs, the structural characteristics of the separated region, and the time required for the development of the separation following onset of an adverse pressure gradient. Here we deal with these issues for a boundary layer that is laminar upstream of the separation, focusing on the unsteady features of the separation and its development in a nominally steady free-stream flow.

The present work, which concentrates on two-dimensional flows, is part of a computational and experimental study of unsteady effects in three-dimensional laminar-boundary-layer separation. This paper describes a numerical study of the time-dependent two-dimensional flow field that develops when a laminar boundary layer is subjected to a sudden, local, adverse pressure gradient. The objective of this work was to obtain new insight to the physics of such flows. For more details see Pauley, Moin & Reynolds (1988).

There is a great deal of prior work on separation, much of it dealing with the steady structure in two or three dimensions (e.g. Gaster 1966; Peake & Tobak 1982). The typical structure of a two-dimensional laminar-boundary-layer separation bubble was described by Horton (1968). Figure 1 shows a sketch of the separation. Near the separation point, the recirculation region contains slow-moving fluid. The centre of the recirculation vortex lies near the reattachment point and the recirculation velocities are stronger in this region. At the point of separation, the dividing

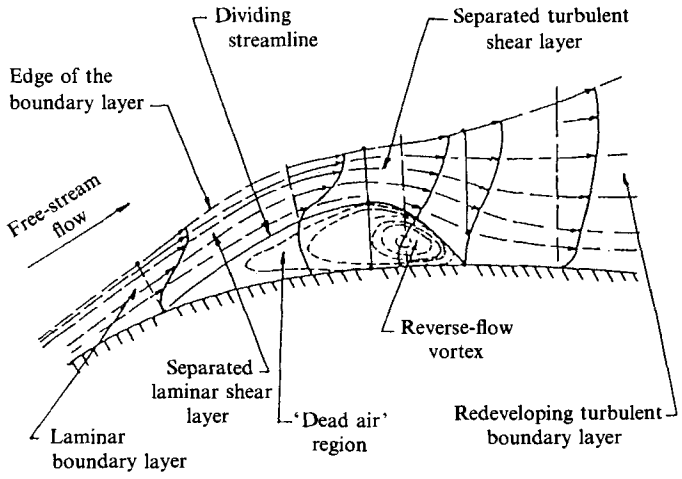

FIGURE 1. The flow field in the vicinity of a transitional separation bubble. (Horton 1968).

streamline is observed to rise slowly away from the wall. After the boundary layer undergoes transition to turbulent flow, the separation streamline quickly reattaches to the wall. Within the separated region, the wall pressure remains constant near the separation point while a strong pressure gradient accompanies the high-velocity region near the reattachment point. Tani (1964) noted that the length of the separated region was reduced as the adverse pressure gradient increased, and suggested that this was due to more rapid transition of the separated laminar boundary layer. These characteristics of laminar separation bubbles have been seen by many investigators, and as we shall show were also seen in the computations.

Various parameters have been proposed for correlating the characteristics of laminar separation bubbles, and these parameters will be useful in comparing the current computations with past experiments. Dobbinga, Ingen & Kooi (1972) proposed a relationship between the momentum-thickness Reynolds number at separation, $(Re_\theta)_{\text{sep}}$, and the separation angle, γ, defined as the angle between the surface and the dividing streamline,

$$\tan\gamma = B/(Re_\theta)_{\text{sep}}, \tag{1}$$

where the subscript sep denotes evaluation at the separation point and B was typically between 15 and 20. Gaster (1966) studied a laminar separation bubble on a flat plate and found that the separation bubble may be either 'short' or 'long'. He proposed a criterion to predict when the separation will be short or long based on the momentum-thickness Reynolds number and a dimensionless velocity gradient (sometimes called a dimensionless pressure gradient and hence denoted by P),

$$P_{\text{avg}} = \frac{\theta^2_{\text{sep}}}{\nu}\left(\frac{\mathrm{d}u_1}{\mathrm{d}x}\right)_{\text{avg}}. \tag{2}$$

Here the velocity gradient is that which would be obtained in an inviscid analysis with no separation, averaged over the length of the separation, which Gaster cleverly measured by tripping the laminar boundary layer to produce a fully attached turbulent boundary layer. Many researchers (e.g. Thwaites 1949 and Curle & Skan 1957) have proposed separation criteria based on

$$m = \frac{\theta^2_{\text{sep}}}{\nu}\left(\frac{\partial u_e}{\partial x}\right)_{\text{sep}} \tag{3}$$

where u_e is the velocity at the outer edge of the boundary layer. Curle & Skan found $-0.171 < m < -0.068$ for the onset of separation.

The present work concentrates on the unsteady features of separation. The time history of separation has been investigated in a few flow visualization and quantitative experiments (e.g. Despard & Miller 1971; Koromilas & Telionis 1980). Two types of temporal features must be distinguished: (i) the development of the separation region (herein called 'separation build-up'), and (ii) the periodic shedding of cross-stream vortices (herein called 'unsteady separation'). Koromilas & Telionis (1980) investigated separation build-up by impulsively bending a flat plate to imposed a sudden adverse pressure gradient on the boundary layer. The separated region started quite thin but quickly grew and developed into a strong vortex near the reattachment point. From their photographs, it appears that this vortex was shed and a new vortex began to develop. As the separated region became large, the separated shear layer underwent transition and the vortex structures were not visible in the resulting turbulent flow.

Analytical studies and other recent computations have already provided some insight into the features of unsteady separation. Stewartson, Smith & Kaups (1982) studied a steady separation bubble using triple-deck theory, and found that a steady separation structure was not possible for sufficiently strong adverse pressure gradients. Subsequently Elliott & Smith (1987) showed that a periodic instability developed for these strong-pressure-gradient cases. Briley (1971) studied steady laminar separation bubbles by numerical computation, and also found that a steady solution was not possible for strong adverse-pressure-gradient cases. He attributed the unsteadiness to a physical phenomenon and not to numerical instabilities. Gruber, Bestek & Fasel (1987) computed a steady separation bubble and then investigated the stability of the separation to a Tollmien–Schlichting wave. The wave amplitude was found to increase within the separation region. Gruber *et al.* considered this as an indication that the separated boundary layer would always undergo transition to turbulence. Recent work by Bestek, Gruber & Fasel (1989) showed that the separation bubble becomes unsteady if a strong external pressure gradient is applied, and attributed the unsteadiness to turbulent transition of the separated boundary layer. The current computations shed additional light on these matters.

2. Problem definition

The computation mirrors the water channel of the companion experiments (see Henk 1990). The laminar boundary layer on one wall (the 'test wall'), developed under zero pressure gradient, was exposed to a sudden local adverse pressure gradient by initiating suction through a port on the opposite wall (the 'control wall'), with the upstream flow held steady. Figure 2 shows the geometry and computed instantaneous streamlines of the flow. Note that the separated region is confined to about 20% of the channel height near the test wall, and hence the response of the boundary layer should be independent of the way in which the adverse pressure gradient was imposed.

In the development below, the channel height and upstream approach velocity are the characteristic scales used to form non-dimensional quantities, which are denoted by capital letters. Lower-case symbols are dimensional quantities. The suction parameter, S, defined as the fraction of the entering flow removed through the suction port, provides a convenient measure of the strength of the adverse pressure

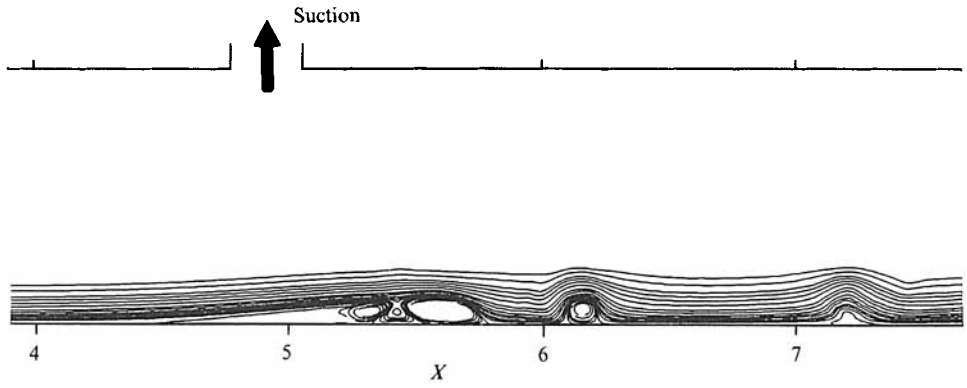

FIGURE 2. Computational domain.

gradient imposed on the boundary layer in the present configuration. Other more general measures will be defined below.

A fractional timestep method developed by Kim & Moin (1985) was used to solve the incompressible Navier–Stokes equations for a fluid with constant viscosity. The method was second-order accurate in space and time.

The inlet flow was prescribed as a Blasius boundary layer of the appropriate thickness under a steady uniform external flow. No-slip boundary conditions were used on the test wall, while no-stress conditions were used along the control wall to reduce the required resolution in this region. A parabolic variation of the suction velocity was used to make the wall-normal velocity continuous along the control wall so as to avoid strong gradients. The initial field was the steady-state solution in the channel with no suction applied. Suction was impulsively applied at $T = 0$.

Various exit boundary conditions were tested, and it was found that the convective exit boundary conditions

$$\frac{\partial u}{\partial t} + c\frac{\partial u}{\partial x} = 0, \quad \frac{\partial v}{\partial t} + c\frac{\partial u}{\partial x} = 0, \tag{4a, b}$$

allowed the propagating vortex structure to exit the domain with minimum distortion. The propagation speed of the vortices within the computational domain gave the value for c. Virtually the same computational results were obtained when the average exit velocity was used for c, and hence the value of c was not critical to the numerical solution.

The basic computations used 256 points in the streamwise direction and 128 points in the normal direction. Half of the grid points were clustered in the boundary layer on the test wall using a hyperbolic tangent distribution. Uniform grid spacing was used in the streamwise direction. The grid-dependence of the solution was tested by doubling the number of points in the streamwise or normal directions; for both cases the changes in the flow velocity and shedding frequency were less than 0.5%.

The timestep for the computations was $\Delta T = 0.005$. To check the timestep independence of the solution, a calculation was run with $\Delta T = 0.0025$. The flow velocities and shedding frequencies for the two step sizes differed by at most 0.5%.

The inlet boundary was set at a location where the inviscid flow field varied by less than 2% from wall to wall across the channel. To test the influence of the exit boundary location, a computational domain was used which was 50% larger and contained 50% more grid points in the streamwise direction, retaining the same grid

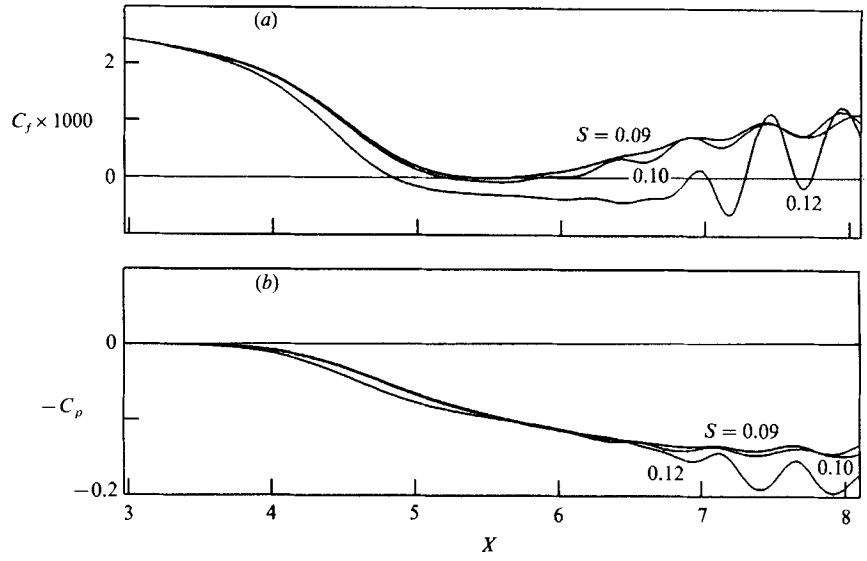

FIGURE 3. Approaching the critical suction strength, $Re_x = 120544$ and $S = 0.09$, 0.10, and 0.12. (*a*) Skin friction, (*b*) pressure coefficient.

	Low speed	Normal speed	High speed
Re_x	59629	120544	238515
$Re_{\delta_{99}}$	1221	1737	2442
Re_θ	162	230	325
U_{sep} (m/s)	0.100	0.203	0.405
θ_{sep} (cm)	0.186	0.132	0.093
f (Hz)	0.37	1.05	2.99
St_θ	0.00689	0.00682	0.00684

TABLE 1. Reynolds numbers and other parameters for the computational cases

spacing. Near the exit of the short domain, the results of the two computations differed by up to 3%, but the results more than one channel width upstream of the exit plane differed by less than 0.2%. Thus, the main results of interest were essentially independent of the domain truncation.

Several different suctions were used at the three Reynolds numbers shown in table 1. The nominal Reynolds numbers listed are based on the conditions at the streamwise location where the suction port begins. Because the velocity outside the boundary layer varies slightly across the channel, the boundary-layer edge velocity used in the Reynolds number and other parameters was taken as the slip velocity on the control wall in the absence of suction, and the boundary-layer thickness parameters were those of the initial laminar boundary-layer on the test wall.

3. Results and discussion

3.1. *Steady separation structure and stability*

In order to determine the effects of the adverse pressure gradient, computations were made for several suction strengths at each Reynolds number. For relatively weak adverse pressure gradients, the separated region built up into a steady, closed

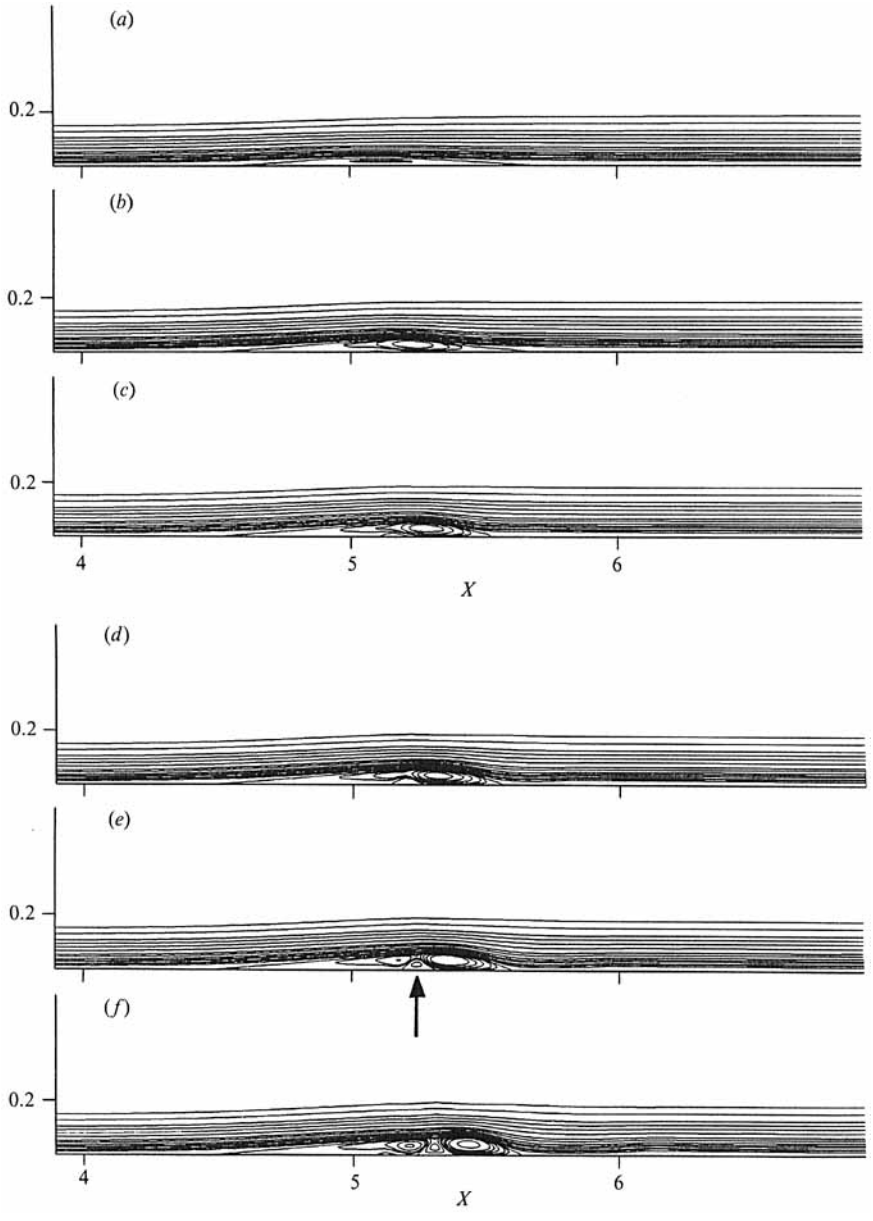

FIGURE 4. Development of separation, $Re_x = 120544$ and $S = 0.22$. (*a*) $T = 2.4$, (*b*) 3.6, (*c*) 4.0, (*d*) 4.4, (*e*) 4.8, (*f*) 5.2.

separation bubble. In each of these cases, the separated region was very thin. For more detail see Pauley *et al.* (1988).

For stronger adverse pressure gradients corresponding to increased suction, the separated region lengthened and small oscillations developed in the skin friction. The instantaneous skin friction and pressure coefficient curves for various suction strengths are shown in figure 3. The oscillations formed near the reattachment point and propagated downstream as 'waves'. The wave amplitude became greater when the pressure gradient was increased. The separation bubble, however, remained steady until vortex shedding began at $S = 0.12$.

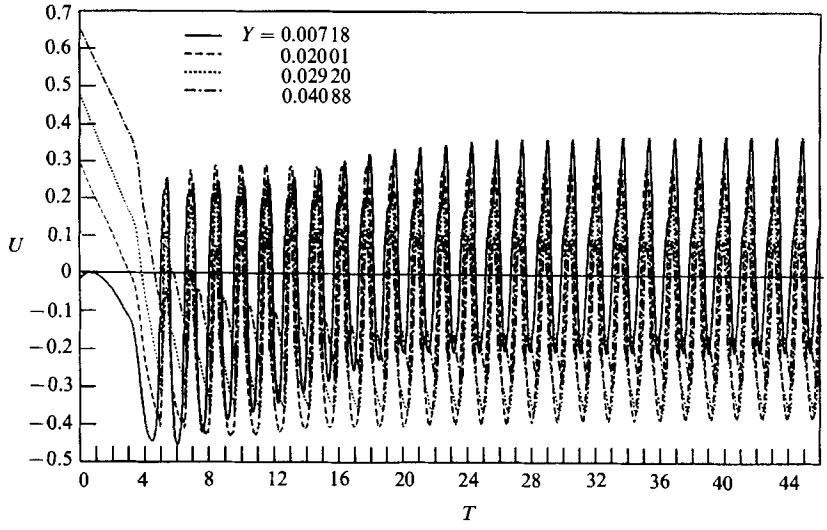

FIGURE 5. Velocity history at $X = 5.36$, $Re_x = 120544$ and $S = 0.22$.

The occurrence of shedding can be observed from the skin-friction curves. Cases where the skin friction was periodically negative (in a limit cycle) are classed herein as 'unsteady separation'. The critical suction strength for the onset of unsteady separation was $S = 0.12$ for all Reynolds numbers tested. Above $S = 0.12$, discrete vortices were shed and additional free-stream fluid was entrained into the separation. These vortices were stronger when a stronger adverse pressure gradient (suction) was applied.

3.2. *Unsteady separation structure*

The unsteady separated structures were examined in detail for the case of $Re_x = 120544$ and $S = 0.22$, for which a strong separation was produced. The streamlines during the separation build-up are shown in figure 4. Initially, the separation is symmetric, reminiscent of a steady separation bubble. As the separation develops, a recirculating region is formed which moves downstream and increases in strength. The separation then pinches into two distinct cells and a small region of counter-rotating fluid forms (indicated by an arrow in figure 4*e*). Throughout the development, the upstream portion of the separation remains steady and quiescent. This separation development is very similar to that seen by Koromilas & Telionis (1980).

To examine the development of the separation, streamwise velocity histories were recorded in the region of vortex shedding at four positions above the wall. These velocity histories are shown in figure 5. The sampling points are at various Y-locations all below the centre of the vortices, hence the histories characterize the near-wall flow. After a brief initial adjustment period, the boundary layer begins to shed periodically at a constant frequency. The magnitude of the velocity oscillations settles to within 5% of the limit-cycle magnitude after 10 oscillations.

A limit-cycle oscillation is reached after the initial separation build-up. Figure 6 shows the streamline structure at six equally spaced intervals in the limit cycle. The flow near the separation point is virtually steady. Fluctuation in the height of the recirculating region indicates that boundary-layer fluid is entrained to allow the continuation of the shedding process. In the limit cycle, the shed vortices are considerably stronger than the first vortex shed after suction is initiated (compare

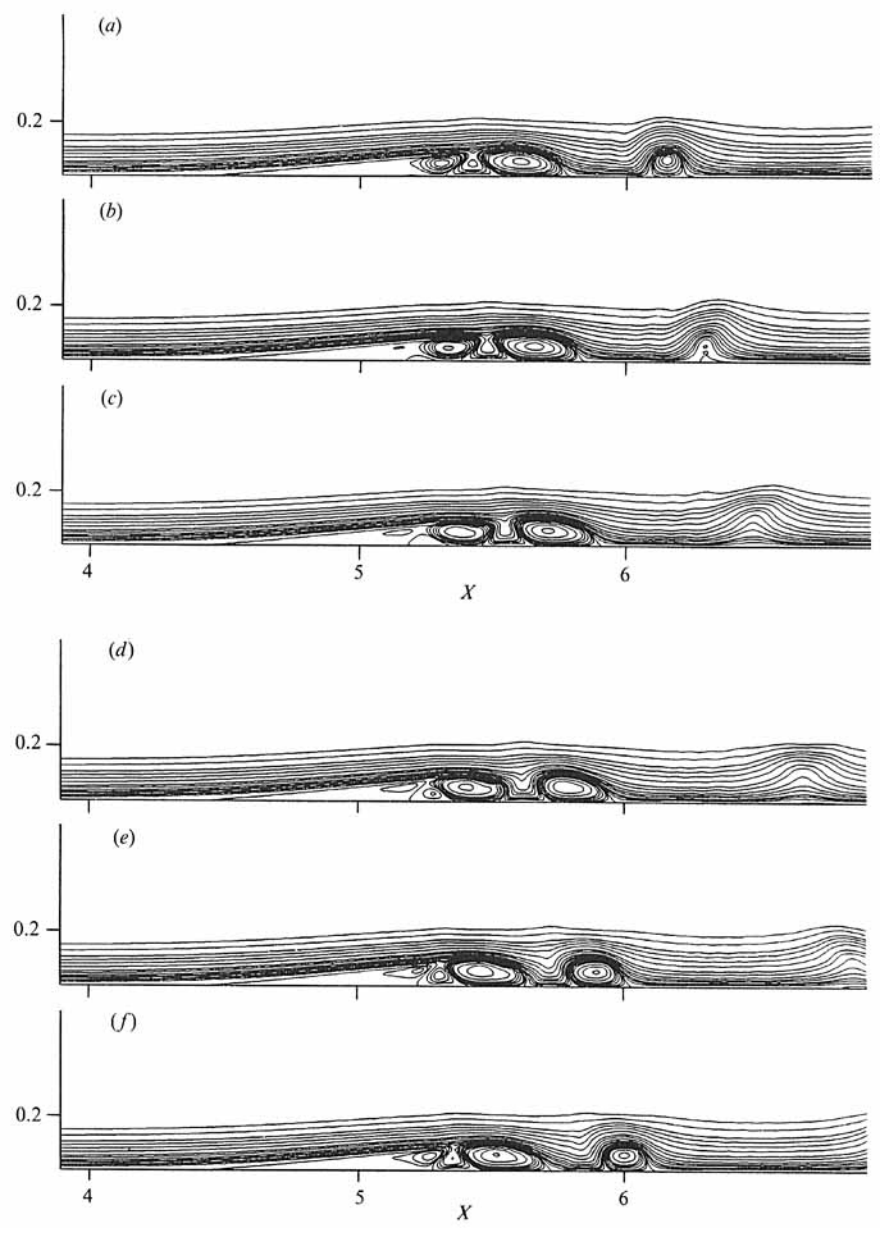

FIGURE 6. Streamlines for limit cycle shedding, $Re_x = 120544$ and $S = 0.22$. (*a*) $T = 43.46$, (*b*) 43.72, (*c*) 43.99, (*d*) 44.25, (*e*) 44.51, (*f*) 44.78.

figure 6 to figure 4). The shed vortices develop an oval shape due to the secondary counter-rotating vortices which cause the primary vortices to be pushed downstream near the wall and pulled upstream away from the wall. As the primary vortices propagate downstream and the secondary vortices lose strength, their shape becomes rounded and the vortices propagate at approximately 65% of the local free-stream velocity.

3.3. *Shedding frequency*

The parameters controlling the vortex shedding frequency were studied by varying the suction strength and Reynolds number. The shedding frequency was determined from the Fourier transform of the velocity histories during the limit-cycle oscillations. At a fixed Reynolds number, the shedding frequency was found to be independent of the suction strength. However, the shedding frequency was different for the three Reynolds numbers.

The shedding frequency was non-dimensionalized with the boundary-layer momentum thickness at separation and the local free-stream velocity to produce a Strouhal number,

$$St_\theta = \frac{f\theta_{\text{sep}}}{(u_e)_{\text{sep}}}. \tag{5}$$

For the three Reynolds numbers examined and all suctions, the Strouhal numbers collapsed very well to

$$St_\theta = 0.006\,86 \pm 0.6\,\%. \tag{6}$$

The results for the three Reynolds numbers and the dimensional quantities which correspond to the companion experiment are presented in table 1. This simple relationship is recommended for predicting the shedding frequency in practical situations; note that the frequency depends only upon the free-stream velocity and momentum thickness at the separation point.

3.4. *Conditions at the separation point*

At the separation point, the flow was very steady throughout the unsteady shedding process (which occurred downstream). Two conditions at the separation point were examined: the separation angle and the Thwaites parameter, (3).

The angle of separation was determined from the simulation and used to calculate the parameter B in (1). B fell in the range 15.5–22.5, and was observed to increase when either the Reynolds number of the pressure gradient was increased. Thus, the observed separation angles were consistent with previous experiments (Dobbinga *et al.* 1972).

Thwaites' (1949) parameter m (see (3)) uses the boundary-layer edge velocity gradient at the separation point. In the current computations, true edge conditions did not exist since the potential flow varied across the channel. Moreover, the value of m was found to be strongly dependent on the distance from the wall where u_e was evaluated. Therefore, in order to obtain a more representative effective edge velocity gradient, the pressure gradient across the boundary layer was neglected and the Navier–Stokes equation was evaluated at the wall to give

$$u_e \frac{\partial u_e}{\partial x} = -\nu \left(\frac{\partial^2 u}{\partial y^2}\right)_{y=0}, \tag{7}$$

whence

$$m = -\left[\frac{\theta^2}{u_e}\left(\frac{\partial^2 u}{\partial y^2}\right)_{y=0}\right]_{\text{sep}}. \tag{8}$$

Thwaites suggested $m \approx -0.082$. Curle & Skan (1957) reported the results of several investigators who found $-0.171 < m < -0.068$. Values from the present investigation were in the range $-0.121 < m < -0.076$. Thus, the observed Thwaites parameters were consistent with experiments.

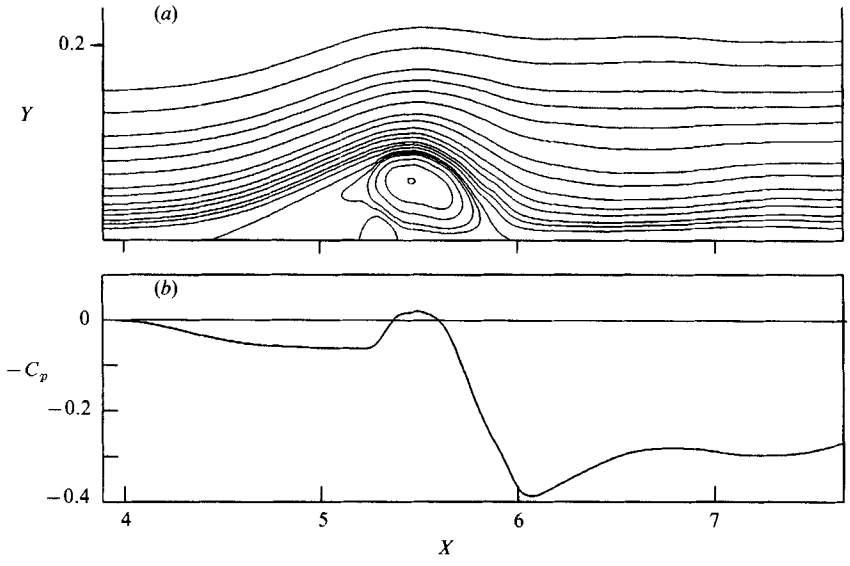

FIGURE 7. (a) Time-averaged streamlines and (b) pressure coefficient, $Re_x = 120544$ and $S = 0.22$. Note that the vertical lengthscale has been stretched by a factor of 5.

3.5. *Time-averaged separation bubbles*

When the unsteady separation was time-averaged over a number of shedding cycles, the average separation was a closed bubble. Shown in figure 7 are the time-averaged streamlines and pressure coefficient at $Re_x = 120544$ and $S = 0.22$. Note the similarity to figure 1. This separated region spans the entire region of the 'inviscid' adverse pressure gradient on the test wall. Near the separation point, slow-moving fluid is contained in the recirculating region and the pressure is nearly constant at the wall. Downstream, a strong recirculation is present in the region of strong pressure gradient. Tani (1964), Gaster (1966), Horton (1968) and others have reported this same structure for the time-average structure of separation bubbles. Similar characteristics near the separation point were predicted theoretically by Smith (1979, 1985).

The separation length, l, taken as the distance between separation and reattachment points of the time-averaged separation, was greatly affected by the presence of unsteady vortex shedding. For a given Reynolds number, the steady separation bubble increased in length when a stronger adverse pressure gradient was applied. After the onset of shedding, the length of the time-averaged separation decreased when the adverse pressure gradient was made stronger. The maximum time-averaged separation length therefore occurred at the onset of shedding.

Similar pressure distributions have been observed by McCullough & Gault (1949). A region of nearly constant pressure was followed by a strong pressure gradient near reattachment. For separation bubbles with this pressure distribution, the length of the separation bubble decreased as the airfoil angle of attack (and hence the adverse pressure gradient) increased. Gaster also found that the separation length of short bubbles decreased as the adverse pressure gradient increased. Thus, the time-averaged structure from the computations strongly resembles that found in experiments.

Gaster observed a 'bursting condition' where the length of the separation bubble suddenly changed. At adverse pressure gradients stronger than the bursting

condition, he found short separation bubbles similar to the time-averaged bubbles found in the present computations for unsteady separation. For short separation bubbles, a constant pressure near separation was followed by a strong adverse pressure gradient at reattachment, similar to the time-averaged pressure distribution of the computations. Just at the bursting condition, Gaster found that the bubble burst to a long bubble with no distinct strong adverse pressure gradient region, similar to the pressure distribution found for steady separation bubbles in the computations. These similarities suggest that Gaster's long and short bubbles were steady and unsteady bubbles respectively.

Gaster recorded the hot-wire oscilloscope signals at different locations in both short and long bubbles. The signal from a short bubble showed a low-frequency component in the fluctuations while that from a long bubble showed no low-frequency component. In the current computations, time-averaged short bubbles were produced by unsteady shedding separation while long bubbles were steady. McCullough & Gault and Gaster attributed their unsteady results to the transition of the separated shear layer to turbulence. The present computations suggest that the observed oscillations arose from periodic vortex shedding.

3.6. *Shedding criterion*

The critical shedding condition $S = 0.12$ developed in §3.1 is useful only in the present geometry. In order to develop a shedding criterion applicable to general flows, one would prefer a criterion based on conditions imposed on the boundary layer by an otherwise inviscid flow through a Thwaites-like dimensionless 'pressure-gradient' parameter,

$$P = \frac{\theta_{\text{sep}}^2}{\nu} \frac{\mathrm{d}u_{\text{i}}}{\mathrm{d}x}, \tag{9}$$

where $\mathrm{d}u_{\text{i}}/\mathrm{d}x$ is an appropriate inviscid velocity gradient along the wall. To test the various options, the momentum thickness was obtained by integrating across the boundary layer at separation; the time-averaged momentum thickness was used in unsteady cases. A potential flow analysis was used to determine the inviscid flow field in the channel with suction, and three different possibilities for the inviscid velocity gradient were explored:

(i) the inviscid velocity gradient at the separation point ($P_{\text{sep}} = m$);

(ii) the inviscid velocity gradient averaged over the length of the separation bubble (P_{avg}); and

(iii) the maximum (negative) inviscid velocity gradient in the separation region (P_{max}). It was found that the best correlation was obtained when the maximum (negative) inviscid velocity gradient encountered along the separation was used, and that

$$P_{\text{max}} = \frac{\theta_{\text{sep}}^2}{\nu} \left(\frac{\mathrm{d}u_{\text{i}}}{\mathrm{d}x}\right)_{\text{max}} \approx -0.24. \tag{10}$$

This is suggested for predicting the onset of unsteady separation in other flow configurations. The characteristics of all computed bubbles are presented in table 2.

Gaster's bursting condition differs in his use of P_{avg}. He found that as $(Re_\theta)_{\text{sep}}$ was reduced there existed a critical condition at which a small separation bubble would 'burst' into a large separation bubble. Studying several different geometries, he found the bursting condition to be dependent on $(Re_\theta)_{\text{sep}}$ and P_{avg}, and presented the critical bursting conditions by a line in a $(Re_\theta)_{\text{sep}}$–P_{avg} diagram. The time-averaged results of the present numerical study were compared with Gaster's criterion by

S	x_{sep} (m)	U_{sep} (m/s)	θ_{sep} (10^3 m)	$Re_{\theta_{sep}}$	l/θ_{sep}	m	P_{avg}	P_{sep}	P_{max}
				$Re_x = 59629$					
0.11	0.657	0.098	1.804	162.9	73.4	−0.076	−0.082	−0.188	−0.209
0.115	0.642	0.098	1.816	165.0	102.8	−0.082	−0.083	−0.217	−0.221
0.118	0.638	0.099	1.823	165.9	117.0	−0.084	−0.080	−0.227	−0.329
0.12	0.638	0.099	1.887	177.1	193.1*	−0.095	−0.054	−0.246	−0.249*
0.14	0.608	0.100	1.862	171.8	177.1	−0.098	−0.070	−0.266	−0.284
0.16	0.593	0.106	1.851	167.9	167.2	−0.102	−0.080	−0.266	−0.320
0.18	0.595	0.100	1.823	167.7	140.1	−0.105	−0.157	−0.298	−0.349
0.20	0.588	0.100	1.813	167.1	78.8	−0.108	−0.293	−0.303	−0.384
0.22	0.580	0.101	1.803	166.6	70.8	−0.112	−0.347	−0.301	−0.418
				$Re_x = 120544$					
0.08	0.656	0.203	1.307	243.3	105.0	−0.083	−0.064	−0.146	−0.161
0.10	0.630	0.203	1.310	244.2	181.3	−0.091	−0.074	−0.170	−0.230
0.11	0.620	0.204	1.343	251.1	196.4	−0.097	−0.082	−0.231	−0.234
0.12	0.622	0.202	1.295	240.6	261.8*	−0.096	−0.064	−0.236	−0.237*
0.14	0.589	0.206	1.324	250.2	181.3	−0.106	−0.107	−0.241	−0.289
0.16	0.590	0.205	1.294	243.1	144.3	−0.109	−0.197	−0.254	−0.316
0.18	0.582	0.205	1.291	242.7	118.1	−0.113	−0.265	−0.261	−0.354
0.20	0.576	0.205	1.283	241.4	89.0	−0.116	−0.339	−0.267	−0.389
0.22	0.572	0.205	1.283	240.9	75.7	−0.117	−0.383	−0.287	−0.427
				$Re_x = 238515$					
0.10	0.635	0.401	0.914	335.4	108.7	−0.087	−0.128	−0.193	−0.194
0.11	0.622	0.402	0.914	337.7	122.9	−0.094	−0.150	−0.213	−0.215
0.115	0.616	0.403	0.917	339.3	143.4	−0.099	−0.151	−0.220	−0.225
0.12	0.605	0.405	0.926	344.8	181.0*	−0.103	−0.174	−0.221	−0.240*
0.14	0.592	0.406	0.926	345.9	141.9	−0.121	−0.221	−0.230	−0.280
0.18	0.576	0.407	0.947	353.9	88.5	−0.121	−0.344	−0.258	−0.377

TABLE 2. Summary of time-averaged computational results. *Indicates onset of shedding.

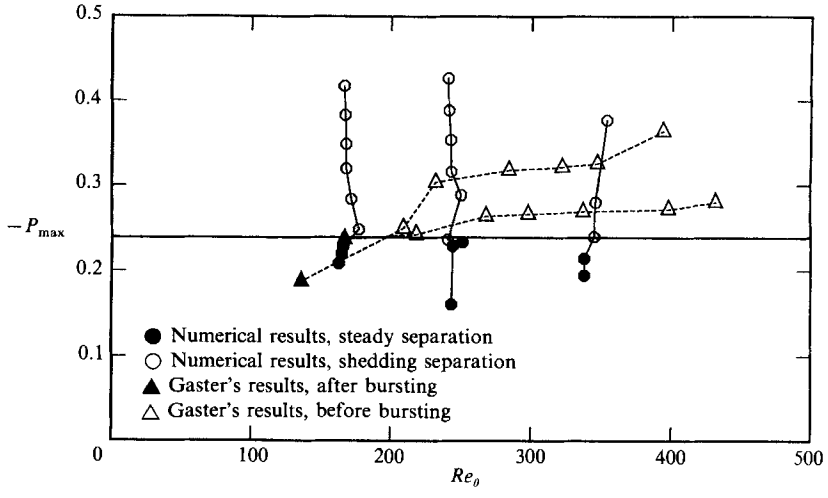

FIGURE 8. Numerical and experimental data approaching the shedding criterion.

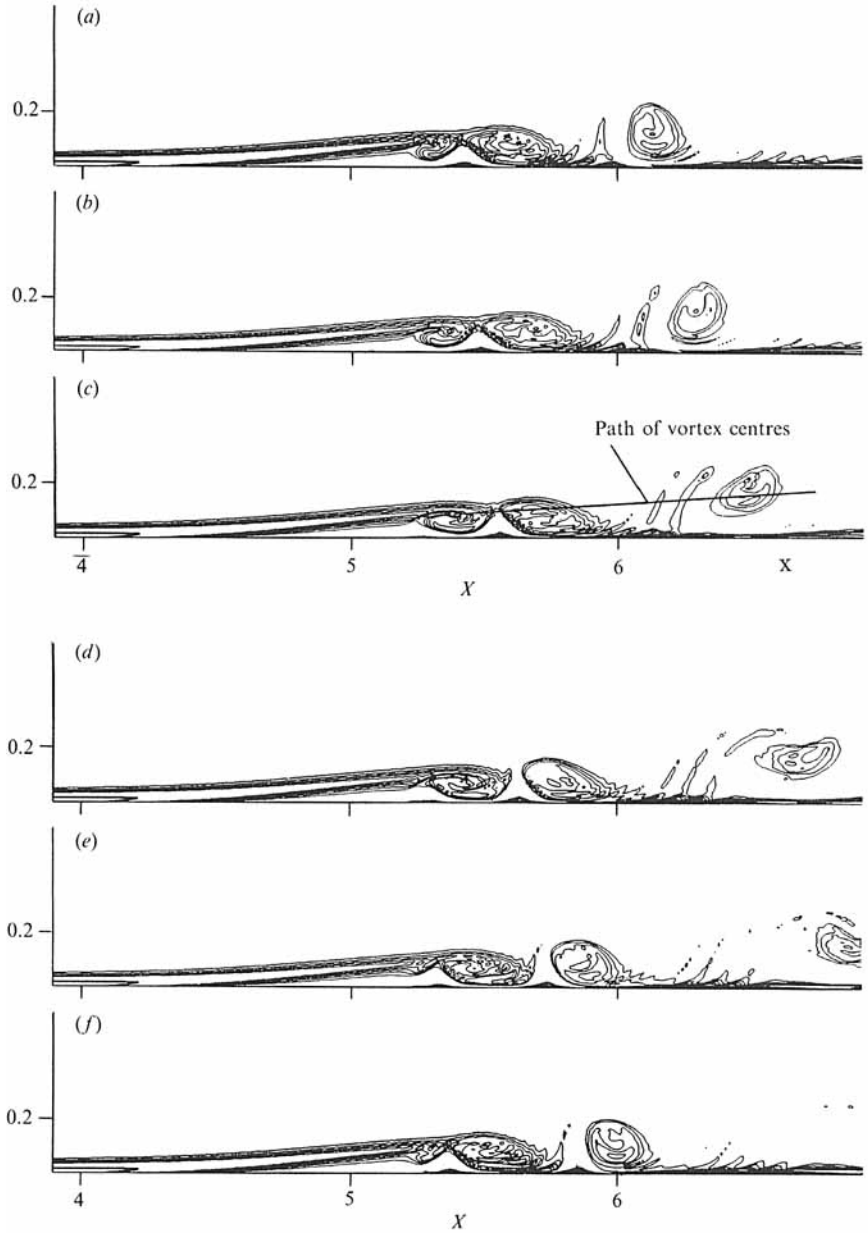

FIGURE 9. Vorticity field for limit-cycle shedding, $Re_x = 120544$ and $S = 0.22$. (*a*) $T = 43.46$, (*b*) 43.72, (*c*) 43.99, (*d*) 44.25, (*e*) 44.51, (*f*) 44.78.

averaging the inviscid velocity gradient across the separation region as he suggested. In all cases his criterion failed to predict bursting, indicating that his bursting line does not characterize the separation observed in the present geometry.

To test Gaster's data against (10), maximum (negative) velocity gradients were extracted from his data. The results from his data and the present computations are shown in figure 8, where each set of cases is connected by a line. Note that Gaster's bursting occurred when $P_{\max} = -0.24$, consistent with (10). We conclude that Gaster's 'bursting' was actually the demise of unsteady separation.

Gaster's bursting line suggests that bursting can occur (i) when Re_θ is decreased while $P_{\max}$ remains constant or (ii) when $P_{\max}$ is increased while Re_θ is fixed. The present criterion predicts the bursting of a short bubble to a long bubble only when $P_{\max}$ is decreased. Although these criteria appear to be in contradiction, it was found that the bursting condition for Gaster's experimental data is predicted by both criteria. The onset of shedding for the current computations, however, is predicted only by the $P_{\max}$ criterion, (10). The $P_{\max}$ criterion is found to be more general and is therefore suggested for predicting the onset of unsteady separation.

3.7. *Vorticity and inviscid linear stability*

In figure 9 it is seen that the vorticity distribution found in the computations is similar to that in a free-shear layer. Shedding occurs from the separated shear layer and the path of the shed vortex follows the centre of the shear layer. The presence of the adjacent wall appears to exert little influence on the propagating vortex. This suggests that vortex shedding frequency might be predicted by a linear stability analysis of a shear layer in the absence of a wall.

Consider a free-shear layer between two streams, u_1 and u_2; the velocity difference across the shear layer is $\Delta u = u_2 - u_1$ and the average velocity is $\bar{u} = \frac{1}{2}(u_1 + u_2)$. The vorticity thickness $\delta_\omega = \Delta u/(\partial u/\partial y)_{\max}$ and the velocity ratio $\lambda = (\Delta u)/(2\bar{u})$ may be used to characterize the shear layer. Following Monkewitz & Huerre (1982), the frequency may be expressed non-dimensionally as

$$\omega^* = \tfrac{1}{4}\delta_\omega \frac{(2\pi f)}{\bar{u}} \tag{11}$$

(also see Michalke 1964). In inviscid analysis of parallel shear flows, the most amplified frequency for a tanh profile is $\omega^* \approx 0.21$ and is not strongly dependent on either λ or the profile shape, so one would expect $\omega^* \approx 0.21$ in the separated region.

To test this idea, the computed velocity field was time-averaged to obtain values of $\delta_\omega(x)$ and $\bar{u}(x)$. Beyond the separation point, the separated region contained virtually stagnant fluid, corresponding to $\lambda = 1.0$. In the unsteady region of the separation, λ and the vorticity thickness changed significantly with streamwise distance and hence the non-dimensional shedding frequency ω^* varied significantly in the streamwise direction. However, at the streamwise location of the centre of the time-averaged vortex (see figure 7), where new shed vortices were observed to form, $\omega^* = 0.21$ was found in all cases. We conclude that the vortices are indeed formed as a result of the inviscid instability of the detached shear layer, and that the shedding frequency is consistent with linear stability analysis.

4. Conclusions

The separation of a laminar boundary layer under the influence of a suddenly imposed external adverse pressure gradient was studied in two dimensions. A strong pressure gradient created periodic shedding from the separation. It was found that the shedding Strouhal number based on the local boundary-layer edge velocity and the boundary-layer momentum thickness at separation was constant, independent of Reynolds number and the pressure gradient. A criterion for onset of shedding was established in terms of a non-dimensional inviscid velocity gradient. This criterion is consistent with experimental results of Gaster. It appears that Gaster's 'bursting' was simply the demise of unsteady separation. Unsteady separation arises from inviscid instability of the separated shear layer.

This research has been supported by the Office of Naval Research under contract number N00014-84-K-0232. Computer facilities were provided by the NAS facility at NASA-Ames Research Center. Three years of financial support for L. L. P. was provided by a fellowship from the National Science Foundation. These contributions are gratefully acknowledged.

REFERENCES

BESTEK, H., GRUBER, K. & FASEL, H. 1989 Self-excited unsteadiness of laminar separation bubbles caused by natural transition. In *The Prediction and Exploitation of Separated Flow*. The Royal Aeronautical Society.

BRILEY, W. R. 1971 A numerical study of laminar separation bubbles using the Navier–Stokes equations. *J. Fluid Mech.* **47**, 713–736.

CURLE, N. & SKAN, S. W. 1957 Approximate methods for predicting separation properties of laminar boundary layers. *Aero. Q.* **8**, 257–268.

DESPARD, R. A. & MILLER, J. A. 1971 Separation in oscillating boundary-layer flows. *J. Fluid Mech.* **47**, 21–31.

DOBBINGA, E., INGEN, J. L. VAN & KOOI, J. W. 1972 Some research on two-dimensional laminar separation bubbles. *AGARD CP*-4, p. 102.

ELLIOTT, J. W. & SMITH, F. T. 1987 Dynamic stall due to unsteady marginal separation. *J. Fluid Mech.* **179**, 489–512.

GASTER, M. 1966 The structure and behavior of laminar separation bubbles. *AGARD CP*-4, pp. 813–854.

GRUBER, K., BESTEK, H. & FASEL, H. 1987 Interaction between a Tollmien–Schlichting wave and a laminar separation bubble. *AIAA*-87-1256.

HENK, R. W. 1990 An experimental study of the fluid mechanics of an unsteady, three-dimensional separation. Ph.D. thesis, Stanford University.

HORTON, H. P. 1968 Laminar separation bubbles in two- and three-dimensional incompressible flow. Ph.D. thesis, University of London.

KIM, J. & MOIN, P. 1985 Application of a fractional-step method to incompressible Navier–Stokes equations. *J. Comput. Phys.* **59**, 308–323.

KOROMILAS, C. A. & TELIONIS, D. P. 1980 Unsteady laminar separation: an experimental study. *J. Fluid Mech.* **97**, 347–384.

MCCULLOUGH, G. B. & GAULT, D. E. 1949 Boundary-layer and stalling characteristics of the NACA 64 A 006 Airfoil Section. *NACA TN* 1894.

MICHALKE, A. 1964 On the inviscid instability of the hyperbolic-tangent velocity profile. *J. Fluid Mech.* **19**, 543–556.

MONKEWITZ, P. A. & HUERRE, P. 1982 Influence of the velocity ratio on the spatial instability of mixing layers. *Phys. Fluids* **25**, 1137–1143.

PAULEY, L. L., MOIN, P. & REYNOLDS, W. C. 1988 A numerical study of unsteady laminar boundary-layer separation. *Rep.* TF-34, Department of Mechanical Engineering, Stanford University, Stanford, CA.

PEAKE, D. T. & TOBAK, M. 1982 Three-dimensional interactions and vortical flows with emphasis on high speeds. *AGARDograph* 252.

SMITH, F. T. 1979 Laminar flow of an incompressible fluid past a bluff body: the separation, reattachment, eddy properties and drag. *J. Fluid Mech.* **92**, 171–205.

SMITH, F. T. 1985 A structure for laminar flow past a bluff body at high Reynolds number. *J. Fluid Mech.* **155**, 175–191.

STEWARTSON, K., SMITH, F. T. & KAUPS, K. 1982 Marginal separation. *Stud. Appl. Maths* **67**, 45–61.

TANI, L. 1964 Low-speed flows involving bubble separations. *Prog. Aero. Sci.* **5**, 70–103.

THWAITES, B. 1949 Approximate calculation of the laminar boundary layer. *Aero. Q.* **14**, 61–85.